

AD-A144 776

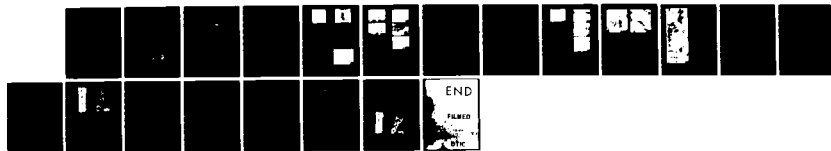
MICROSCOPIC ASPECTS OF WEAR PROCESSES IN METALS(U)
NATIONAL BUREAU OF STANDARDS WASHINGTON DC METALLURGY
DIV A W RUFF ET AL. 01 APR 82 N00014-80-F-0032

1/1

UNCLASSIFIED

F/G 20/11

NL





MICROCOPY RESOLUTION TEST CHART
NATIONAL BUREAU OF STANDARDS-1963-A

2

AD-A144 776

MICROSCOPIC ASPECTS OF
WEAR PROCESSES IN METALS

A.W.Ruff
P.J.Blau

Metallurgy Division
Center for Materials Science
National Measurements Laboratory
National Bureau of Standards
U.S. Department of Commerce
Washington, DC 20234

Jan. 1, 1981 - Dec. 31, 1981
Annual Report
N00014-80-F-0032
NR 091-011

April 1, 1982


Prepared for:
Office of Naval Research
Department of the Navy
Arlington, VA 22217

DTIC
ELECTE
S AUG 17 1984 D
L7

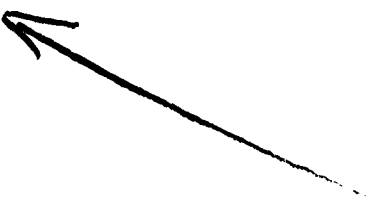
This document has been approved
for public release and sale; its
distribution is unlimited.

DTIC FILE COPY

Abstract



The three articles grouped in this document include the following topics: sliding wear behavior of electron beam ~~etched~~ surface melted O-2 tool steel; the wear-in process during the sliding of copper alloys against 52100 steel; and interpretations of the friction and wear break-in behavior of metals in sliding contact.



SLIDING WEAR BEHAVIOR OF ELECTRON BEAM SURFACE MELTED O-2 TOOL STEEL

A. W. Ruff and L. K. Ives
Metallurgy Division
National Bureau of Standards
Washington, D.C.

ABSTRACT

Studies were carried out on the dry sliding wear behavior of electron beam melted surface layers on a type O-2 tool steel, and on annealed and conventionally hardened O-2 steel specimens for comparison. Wear tests were conducted in a flowing argon atmosphere at a sliding speed of 20 cm/s, a load of 10 N, and against a 52100 bearing steel ring. Wear surface morphology was studied along with subsurface structure using optical and electron microscopy methods. The study concentrated on the wear of this steel after different processing treatments. Electron beam surface melting and subsequent rapid solidification *in situ* of the steel produced a highly refined martensitic microstructure having higher hardness values and better wear resistance than obtained using conventional quench hardening of that steel. Carbide distribution and martensite phase morphology were affected by this surface melting process; those microstructural characteristics influenced the wear behavior. Variations in electron beam power and surface speed during melting were explored in terms of their effect on the resulting surface layer. The wear test system used was computer interfaced and controlled, permitting continuous measurements of wear depth and friction force.

1. INTRODUCTION

There is considerable interest (1) in the development of wear-resistant coatings and surface treatments for metals used in service under a variety of different conditions. These conditions include lubricated environments, dry sliding applications and abrasive wearing conditions, among others. Many techniques have been developed to apply suitable coatings on metal substrates or to otherwise modify surfaces, including chemical deposition, physical deposition, diffusion coatings, and most recently techniques of surface modification using directed energy sources such as electron beams and lasers. A number of potential advantages are associated with these surface modification methods (2), among them are the control of the microstructure of the modified near-surface material and the relative lack of interface weaknesses that frequently lead to failure problems (3). This paper will describe experiments using a modified commercial electron beam system for surface modification through melting and rapid solidification *in situ* of surface layers on O-2 tool steel specimens. Wear studies were carried out under dry sliding conditions on the surface melted specimens and on conventionally processed specimens of the same alloy. A significant reduction in wear rate for O-2 steel was found to result from the electron beam surface melting process applied in the present study and is ascribed to the microstructure that resulted from this processing treatment. Relatively few studies of the wear characteristics of rapidly solidified surface layers have been reported

previously (4).

II. EXPERIMENTAL METHODS

A. Wear Test System

A variable speed electric motor with a replaceable 52100 steel wear ring attached to the motor shaft provided sliding motion for the wear test. A test specimen was loaded on top of this ring and was held in place on an instrumented arm which was free to pivot in a vertical plane. Two interchangeable specimen holders were designed for use with the arm; one for rectangular block specimens (6.3 mm x 12.7 mm x 5.4 mm) and one for cylindrical specimens. The holders were designed so that weights could be placed over the contact in order to vary the load. A load of 10 N was used in all tests on the rectangular block specimens that are reported in this paper. Tests were conducted at normal ambient temperature of about 25°C. An enclosure around the contact region was used to maintain a flowing argon atmosphere and a humidity level of about 30% R.H. during the wear tests. A cam operated switch on the wear ring holder was used to synchronize data sampling with the wear ring position to reduce variation due to the ring surface run-out. Digital data sampling took place once each cycle of rotation. Normally ten successive data points were averaged together.

The electronic data acquisition system used measured three parameters; friction force, contact displacement and temperature in a repeating cycle at a 2Hz rate. Contact displacement was measured with a linear variable differential transformer (LVDT) which monitored the change in height of the pivoting arm bearing the specimen holder. Friction force was monitored through the use of two strain gauges attached to the pivoting arm; the resulting signal was directed to an amplifier. Temperature was measured by a thermocouple placed within the enclosure (and in some cases welded to the block specimen). Time was determined using the controlling computer's internal clock. The peripheral devices were wired to an electronic switch scanner (25 Hz reading rate) whose output was directed to a programmable digital voltmeter. Digital data were then fed to a minicomputer. The computer was programmed to select a scanner channel, set the range and operating mode of the voltmeter, and then read a variable value from the voltmeter. Computer software started and stopped the test and carried out preliminary steps of data processing prior to data storage on magnetic disks. Software was developed to plot friction coefficient and displacement *vs* time (sliding distance), calculate and plot wear volume *vs* time. The wear displacement and wear volume plots could be made with either the raw data or after averaging successive groups of eleven data points for smoothing.

B. Electron Beam Melting System

A modified commercial electron beam vacuum welding apparatus (Fig. 1) was used to melt and produce a

RECEIVED
COPY
INSPECTED

A-1

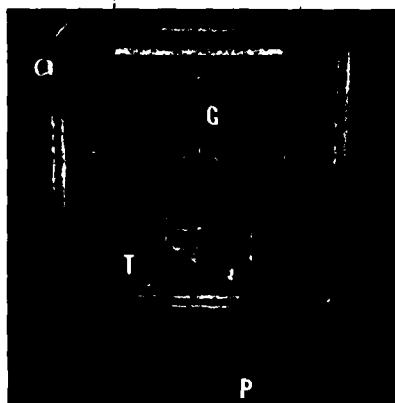


Fig. 1 Electron beam vacuum chamber containing electron gun (G), specimen table (T) and control panel (P).

rapidly solidified surface layer on the 0-2 steel blocks. The electron gun consisted of a tungsten filament cathode, a control grid electrode, an anode and a magnetic focus coil. The beam voltage was normally 20 kV. The working vacuum was about 1 Pa. The specimens to be surface melted were mounted on a rectangular scanning table driven by motors from outside the chamber. The surface melted region was formed by a series of scans moving the specimen under a stationary electron beam of diameter about 0.5 mm in these experiments. Each pass overlapped the previous one to obtain a more uniform melt depth. Rapid solidification of this molten region occurred after the electron beam had passed. When the melting process was completed the surface of the block was uneven (Fig. 2). Prior to wear testing the surface was ground flat, removing about 0.4 mm of material and finished in the manner described below.

C. Test Specimens

Type 0-2 tool steel is a hypereutectoid steel having a composition of 0.9%C, 1.6%Mn, 0.25%Si. The annealed microstructure is composed of carbide spheroids in a ferrite matrix (Fig. 3). Some banding of carbide particles was noted in the original, commercial bar stock material. The specimen blocks were precision ground for wear testing; for good alignment all surfaces were made flat and all sides parallel. The surfaces to be tested were final ground with wet 400 and 600 grit paper, then polished dry with 600 grit microcloth. This gave a surface roughness of about 75nm (R_A) on all specimens. The annealed material had a Knoop hardness value of about 200 (KHN). The quench-hardened material (800°C, followed by 1 hr temper at 275°C) (5) had a hardness value of about 730 KHN. The hardness of the electron beam melted steel varied from 600 KHN to 800 KHN throughout the melted region as will be discussed later.

D. Wear Testing Procedure

Prior to wear testing, the ring and the block specimens were thoroughly cleaned in an ultrasonic cleaner using hexane followed by acetone. The 52100 steel ring (HRC=62) and the specimen block were then fastened in place and the alignment of the block to the ring was adjusted using a small light to illuminate the contact area from behind. A glass slide was positioned below the contact to catch loose wear debris particles. When the specimen was properly aligned, flowing argon was introduced into the chamber. After about 10 minutes of argon flow, the test was begun.

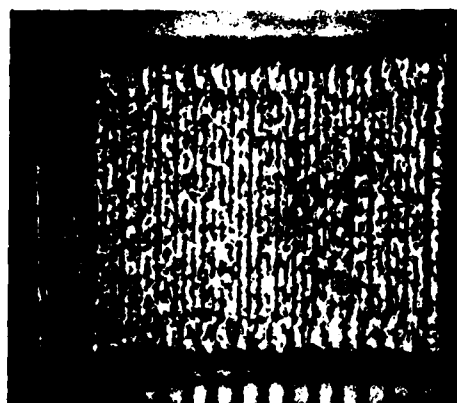


Fig. 2 Electron beam surface melted tool steel specimen block. Scanning direction is vertical. Note millimeter scale at bottom of photograph.

When the test was completed, the specimen and wear debris collected were removed. The ring was cleaned whenever a new type of specimen was tested or when the rings began to show noticeable wear. Typically two or three tests were conducted on one ring.

E. Microscopy Methods

Optical microscopy and scanning electron microscopy (SEM) studies of the worn surfaces, wear debris, and metallographically prepared sections were carried out on a number of specimens. Sputtered coatings of Au-Pd were deposited on the SEM specimens to minimize charging problems in the microscope. Transmission electron microscopy (TEM) studies were carried out to characterize the microstructure resulting from the three processing treatments, and to examine the structure below the wear surface on the electron beam surface melted specimens. The TEM specimen preparation method was similar to that described by Hogmark, Swahn and Vingsbo (6). A 1 mm thick layer of nickel was electrodeposited over the block surface containing the wear scar after cleaning it ultrasonically in acetone to remove loose debris. A conventional nickel sulfamate plating bath (7) was used. Plating was carried out at a current density of 43 A/cm² and a bath temperature of 50°C.

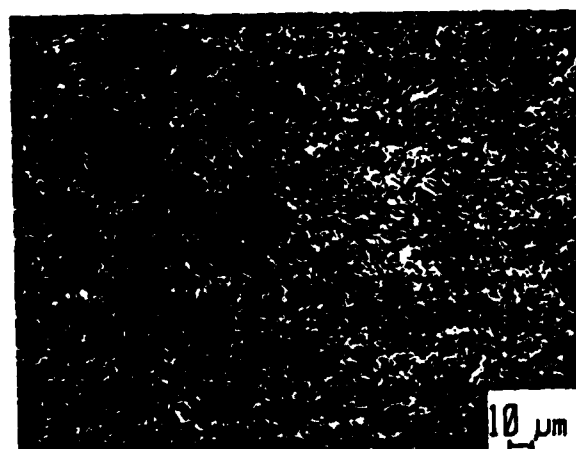


Fig. 3 Microstructure of annealed 0-2 tool steel specimen, etched in nital for 10 seconds.

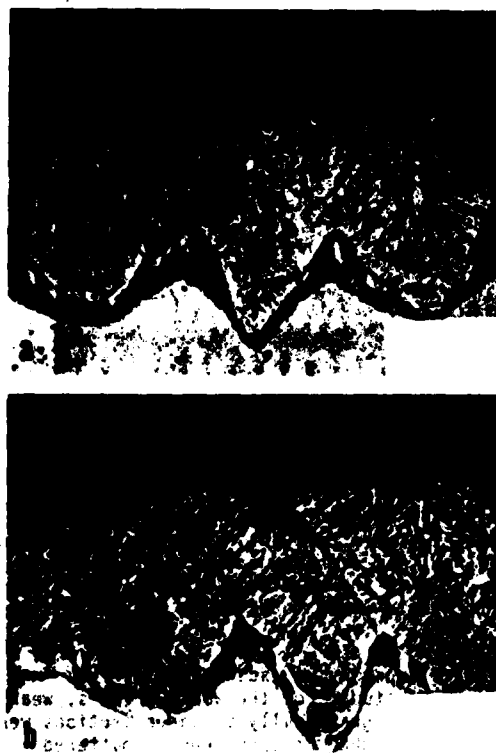


Fig.4 Cross-section view of electron beam melted specimen. (a) central region, (b) end region of melted zone. Etched in nital for 10 seconds.

A thin slice, 0.3-0.4 mm thick, oriented perpendicular to the worn surface was electrodischarge machined from the composite specimen. A 3 mm diameter disk having the wear scar at its center was then electrodischarge machined from this slice. Initial thinning of the disk was carried out by electropolishing in a solution of 10% perchloric acid and 90% acetic acid. Argon ion beam milling was used as the final thinning step. Care was taken to avoid heating of the specimen disk above 50°C during thin foil preparation.

III. RESULTS AND DISCUSSION

A. Electron Beam Surface Melting

The microstructure resulting from electron beam surface melting was characterized and compared with the microstructure of O-2 tool steel in both the annealed, and the quenched and tempered conditions. One example of a cross-sectioned, metallographically polished, and etched surface of an electron beam melted specimen is shown in Fig. 4. The optical photographs show the central region and one end region from a melted length of about 1.3 cm. The melted and solidified zones corresponding to individual scans of the specimen under the electron beam can be recognized. The average melt depth of about 1 mm was achieved in this case under the conditions of 500 watts beam power and a specimen scanning speed of 7.3 cm/sec. The width of a single melt pass at the surface was about 1.5 mm and the overlap of adjacent melt passes was adjusted by spacing the scans about 0.5 mm apart. Higher magnification optical photomicrographs are shown in Fig. 5. The directionally solidified

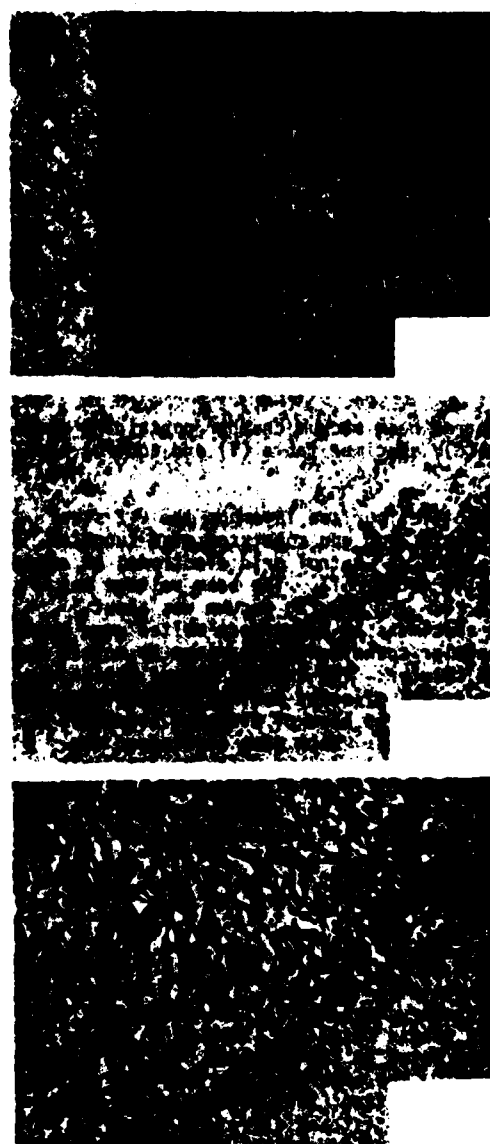


Fig.5 Cross-section of electron beam melted specimen. (a) central region, near depth used for wear testing, (b) central region, base of melt pool (original microstructure at bottom of photograph) (c) end region, base of melt pool. Etched 8 sec in nital.

microstructure characteristic of radial heat flow and solidification of the central region of each melt pass at a depth of about 0.5 mm is shown in Fig. 5a. As a result of the increasing average temperature of the entire specimen block as the scanning process continued under the electron beam, the final microstructure varied from the first pass to the last. Figures 5a, b are taken from near the center of the scanned region (see Fig. 2). Figure 5b shows the microstructure near the melt interface boundary with the unmelted steel, at a depth of about 1 mm. Typically the interface showed no evidence for voids or second phase particles so long as melting conditions were properly chosen.

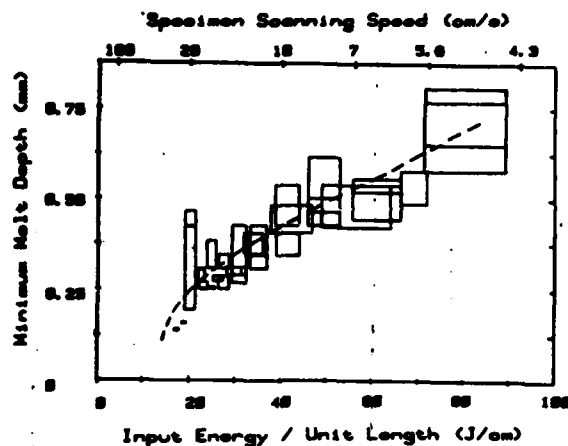


Fig. 6 Variation of minimum melt depth with specimen surface scanning speed (for 400 watt beam), and with input energy per unit length. Rectangles indicate ranges of observed values.

In contrast to this structure, a similar region at the end of the scanned area where the block has a higher average temperature is shown in Fig. 5c. There the different appearance of the martensitic structure after etching is due to the tempering effect experienced during the final cooling stages of the melted/solidified volume. The original spheroidized carbide structure of the block can be seen in areas below the melted material.

A number of experiments were conducted to explore the effect of different surface scanning speeds on the resulting solidified structures. Figure 6 shows the measured relationship between minimum melt depth with surface speed and energy input per unit length (for a 400 watt beam). The maximum melt depth is about twice as large and would correspond to the depth for a single pass. The range in melt depth values is shown by the height of the rectangle plotted that contains the actual measured values. This range is due to fluctuations (e.g. beam power) from pass to pass and the gradually increasing block temperature. The variation in input energy per unit length shown by the width of the rectangle plotted is due to fluctuations in the beam power and scanning speed. There is an approximately linear relation between input energy per unit length (beam power/scanning speed) and melt depth over the region of interest.

Measurements of the microhardness of the melted regions were carried out on cross-sections of several specimens. Figure 7 shows the results of Knoop microhardness determinations plotted against surface scanning speed. For each specimen at a given scanning speed there was a range of microhardness values corresponding to different locations in the melted volume. The curve marked average indicates the observed trend of increased hardness with increased surface scanning speed for locations in the middle of the melt depth. Maximum hardness values of about 800 KHN were observed near the bottom of the melted layer; these are larger than those measured on the bulk quenched and tempered steel specimens. In

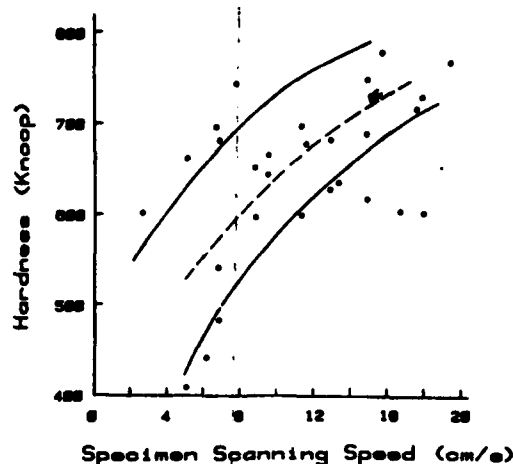


Fig. 7 Measured microhardness (Knoop) vs specimen surface scanning speed (400 w beam power). Scatter results from variation in hardness found through the melted volume.

general the hardness values increased with specimen scanning speed, probably as a direct result of the faster solidification rates associated with the higher scanning speeds.

Studies of the electron beam melted regions indicate a highly refined microstructure in general, although the details observed depend on location within the specimen block, due to variations in pre-heating (from previous electron beam scans on the same block) and solidification rate (melt depth and input beam energy). A distribution of small carbide particles at close spacing was observed. A distribution of martensite plate size was also seen that ranged from fine to coarse depending of the conditions of the melting process. These observations are consistent with the known metallurgy of this tool steel (8). Previous work by Strutt et al. (9) and Kim et al. (10) on a laser melted M-2 tool steel also found a refined, high hardness microstructure to result from laser surface melting.

B. Wear Testing

Wear measurements were made on the O-2 tool steel in an annealed condition, a quenched and tempered condition, and an electron beam surface melted condition. Table I gives the observed wear volume and wear rate data along with the final friction coefficient and the sliding distance for each experiment. The variation in friction and wear displacement during typical tests is shown in Fig. 8 for an electron beam melted specimen. The friction coefficient curve (FC) varied somewhat from test to test; in some cases an initial peak was found, in other cases a more gradual rise was measured. In all cases the friction coefficient was nearly constant after 300-400 m of sliding distance. The wear depth curve (W) in Fig. 8 was also typical. The wear volume curve (WV) represents the wear volume per unit length of wear scar. Figure 9 shows the results of

Table I. Wear and friction results for three conditions of 0-2 steel.

Specimen Type	Sliding Distance* (m)	Pin Friction Coefficient	Wear Volume (mm ³)	Wear Rate* (10 ⁻⁴ mm ³ /m)
Annealed	363	0.48	0.060	1.9
	363	0.53	0.066	2.3
	363 (N)	0.48	0.043	1.2
	363	0.52	0.051	1.4
	363 (N)	0.45	0.030	1.1
	726 (N)	0.53	0.11	1.6
	726 (N)	0.52	0.080	1.3
	726	0.52	0.12	1.7
	726	0.50	0.091	1.2
	avg	0.50	-	1.6
Quench hardened and tempered	363 (N)	0.68	0.032	0.88
	363 (N)	0.84	0.030	0.83
	363 (N)	0.62	0.042	1.1
	363	0.70	0.044	1.2
	726	0.77	0.092	1.3
	726	0.77	0.090	1.2
	726	0.61	0.104	1.4
	avg	0.74	-	1.1
Electron beam surface melted	363 (N)	0.72	0.024	0.66
	363	0.92	0.021	0.58
	363	1.02	0.026	0.72
	726 (N)	0.92	0.062	0.85
	726 (N)	0.94	0.092	1.2
	726	0.88	0.073	1.0
	avg	0.90	-	0.82

*N signifies new ring.

† Wear volume/total sliding distance.

one wear test on an annealed 0-2 steel specimen where the wear volume curve (MV) increased with sliding distance in a nearly constant manner. The friction coefficient value there was considerably lower than for the electron beam melted specimens (Fig. 8). An example of the wear test results for a quenched and tempered specimen is shown in Fig. 10. In this case the wear curve was not smoothed as in the previous figures; the magnitude of fluctuations in the contact position can be seen. The wear volume increased approximately linearly with time. Measurements of the specimen temperature during a test using a thermocouple

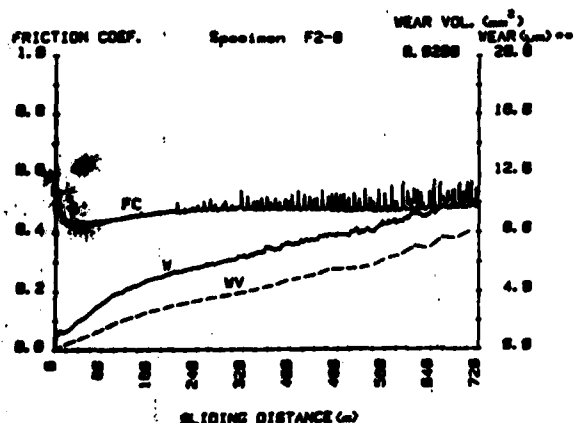


Fig.9 Friction coefficient (FC), wear (W), and wear volume (MV) curves for an annealed 0-2 tool steel specimen.

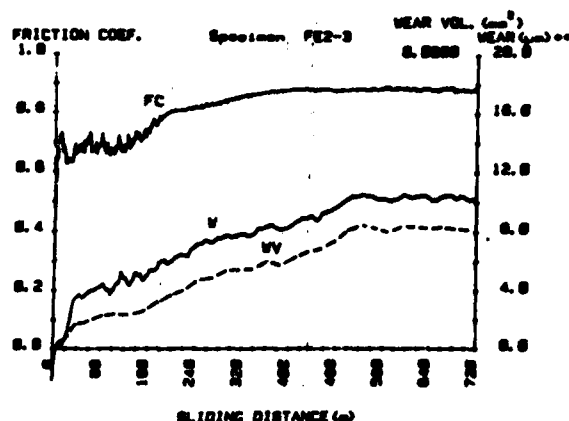


Fig.8 Friction coefficient (FC), wear (W), and wear volume (MV) curves for an electron beam melted specimen of 0-2 tool steel.

welded to the surface about 1 mm from the contact indicated that, typically, the temperature rise was no more than 3°C above the ambient value.

Table I shows that several significant differences were found between the differently processed specimens. The steady state wear rate was reduced about 30% in the quenched and tempered steel when compared to the same alloy in the annealed condition. Further, the electron beam surface melting treatment produced an additional reduction of about 25% relative to the bulk quenched and tempered steel. It is interesting that the friction coefficient values increased from 0.50 to 0.74 in the first case, and from 0.74 to 0.90 in the second. The cause for the friction coefficient changes is not understood but may have resulted from small chemical changes near the surface that the processing treatments produced. The cause for the wear rate changes shown in Table I is attributed to significant changes in the specimen microstructures that are discussed next. The electron

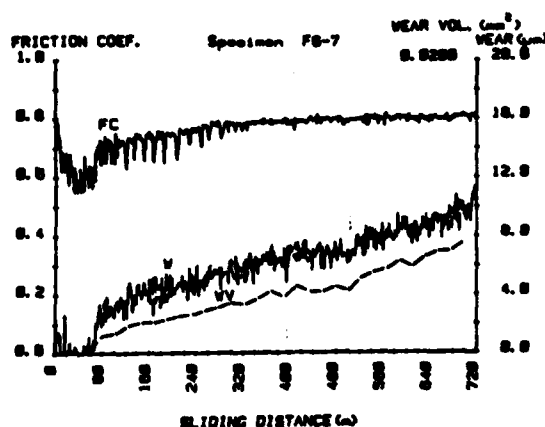


Fig.10 Friction coefficient (FC), wear (W), and wear volume (MV) curves of quench hardened and tempered 0-2 tool steel specimen.



Fig.11 Example of wear scars on electron beam melted block subjected to four tests. Note millimeter scale at bottom. Sliding direction of ring surface shown by arrow.

beam melting treatment, while leading to the highest friction coefficient, also produced a microstructure with more wear resistant characteristics.

C. Specimen Microstructures

An example of a set of wear scars produced on one electron beam surface melted specimen is shown in Fig. 11. Cross sections and taper sections were made of several wear specimens by cutting through the middle of the test block, mounting and metallographically polishing the resulting surface. Figure 12 shows SEM photographs of a taper section (5 deg. angle) produced on a worn electron beam melted specimen in the area of one wear scar. Figure 12a shows the wear scar at the surface (between the dashed lines) in the taper section view; note that due to the taper effect, distances perpendicular to the trace of the surface represent about 10 x magnification of distances in a direction perpendicular to the specimen surface. Figure 12b at a larger magnification indicates the substructure beneath the worn surface. In Fig. 12c one can recognize the martensite and carbide distribution in the electron beam melted material seen before (Fig. 5). Recall that the as-melted surface was ground to a depth of about 0.4 to 0.5 mm prior to wear testing. Hence the substructure at that level corresponds to about the middle of a melt pool, such as is shown in Fig. 5a. The microstructure near the wear surface (arrow) appears disrupted over a region about 1 μ m deep. Etching with 2% nital for 8 seconds revealed numerous small (< 1 μ m) features below the wear surface that appeared as depressions, possibly cavities. It is believed that these features arise from roughness in the wear surface and are accentuated in taper section views. The martensitic microstructure of the steel in this case appears to localize the actual wear damage very near the contact surface, as is brought out in the TEM results from the wear scar areas to be discussed next.

Transmission electron microscopy studies were carried out on each of the three types of specimens. The annealed specimen microstructure consisted of large, spheroidal carbides of the cementite structure (according to electron diffraction data) in a ferrite matrix (Fig. 13). Some of the large carbides remained after the quench and temper treatment was applied to the second group of specimens. As seen in Fig. 14, the structure also contained tempered, twinned martensite. Tempering of the martensite was evidenced

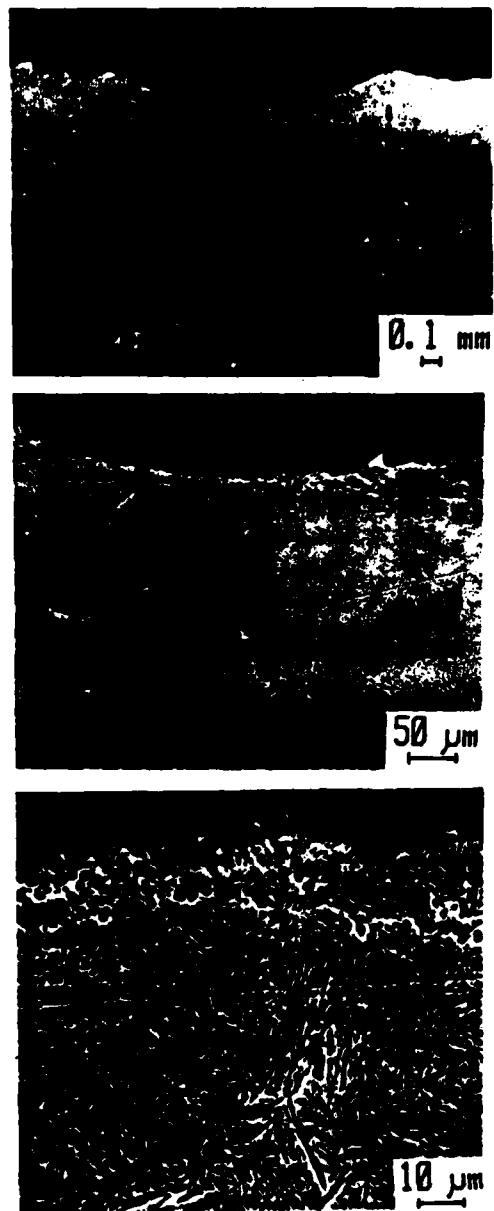


Fig.12 Taper section (5 deg angle) of etched microstructure below wear track in electron beam melted specimen. (a) wear track located between dashed lines, (b) central track region, (c) near-surface structure. Etched 8 sec in nital. Sliding direction of counterface indicated by arrow.

by the presence of fine, epitaxial carbide precipitates throughout.

A cross-section through a wear track in the electron beam surface melted material is shown in Fig. 15. The sliding direction is indicated by the arrow. The material to the left of the line(s) representing the wear surface trace in these electron micrographs is electrodeposited nickel that was used to protect the surface during preparation of the thin



Fig.13 Transmission electron micrograph from an annealed 0-2 tool steel specimen. Large spheroidal carbides and a relatively undeformed ferrite matrix were characteristic.

foil section. This set of micrographs indicates the type of structure that was typical of all thin sections studied from four different wear tracks on these specimens. To the right of the wear surface trace one sees the microstructure typical of the electron beam melted material. It consisted of tempered, twinned martensite. None of the original large carbides were found. The region below each wear track was carefully examined to identify the damage zone and any features resulting from wear. As shown in Fig. 15 the worn surface appeared very smooth in all the sections studied at these relatively high magnifications. Optical and SEM results from the worn surfaces also indicated some regions appearing relatively smooth and polished. Other regions (see Fig. 12) within the wear scar showed a roughened surface, however. There were some indications in the TEM results of damage located very close below the wear surface. Some twinned regions in the martensite such as at A in Fig. 15 appeared bent in the sliding direction. However, the evidence found indicates the deformation damage extended no further than about 50 nm deep from the surface. This finding is consistent with the relatively hard (Knoop hardness 800 or greater), fine structured alloy that resulted from electron beam surface melting and rapid solidification. It is possible that the specimen preparation methods used here might have removed some material unintentionally from the wear surface; further experiments are planned to explore this possibility. Examination of the wear debris produced showed the presence of both metal and oxide particles. The particles were relatively small, less than 0.5 μm, and the larger ones may have been formed by combination of smaller particles. The water vapor content of the argon atmosphere used probably contributed to the oxidation process during wear.

— The findings discussed above indicate that the



Fig.14 Transmission electron micrograph from a quenched and tempered 0-2 tool steel specimen. Some large carbides (A) remained but the characteristic structure was a tempered, twinned martensite.

lower wear rate of the electron beam surface melted alloy resulted from the higher hardness, finer microstructure material produced by this process. Wear involved the removal of both surface oxide and small metallic debris particles. Deformation damage in the bulk material was confined to very near the worn surface.

Budinski (12) has previously discussed the wear of several types of tool steels including 0-2. He has indicated that both metal-to-metal wear (including oxidative wear) and abrasive wear are found to be the principal modes of wear in service. He notes that there is little quantitative information on microstructural effects in wear. Hirst (13) has stated that wear under dry conditions is controlled to a large extent by the oxide-forming characteristics of the steel and that certain tool steel alloys may provide low wear rates due to their particular oxidation characteristics. Others have also observed (14,15) the importance of oxide rubbing and formation effects as well as the transfer of such films between surfaces on the mild wear of steels. Recently, Clayton (16) has identified certain microstructural aspects of steels, namely the pearlite volume fraction, as being significant in affecting wear rate for certain steels. However, it was noted that many other microstructural features may also play a significant role in wear. The results of the present work suggest that the type, size and distribution of phases present in this steel are very important to dry sliding wear performance, at least under loads in the range studied.

IV. CONCLUSIONS

The application of electron beam surface melting and the subsequent rapid solidification in situ



Fig.15 Transmission electron micrograph showing a cross-section through a wear track in the electron beam surface melted O-2 tool steel.

Table II. Summary of Results on Steels Studied

Alloy	Hardness (HRC1000)	Hardness Ratio	Friction Coefficient	Wear Rate ^a (mm ³ /m)	Wear Ratio
1015*	180	1.3	0.80	8.2×10^{-4}	5.1
O-2 (ann.)	230	1	0.50	1.6×10^{-4}	1
O-2 (hardened)	730	0.32	0.74	1.1×10^{-4}	0.69
O-2 (e-beam)	800	0.29	0.90	0.82×10^{-4}	0.51

*listed for comparison purposes; see Ref. 11.
^awear volume/total sliding distance.

produced a substantial change in the microstructure of the O-2 tool steel and also in its wear performance under dry sliding conditions. The wear and friction results are summarized in Table II along with microhardness measurements on these specimens. It is seen that the surface melting process increased the hardness about 10% and the wear resistance about 25% relative to the usual quenched and tempered material. The gain in wear resistance was about a factor of 2 relative to the annealed material. It is thought that the highly refined microstructure resulting from the rapid solidification after surface melting led to this improved wear resistance.

ACKNOWLEDGEMENTS

The preparation of the electron beam surface melted specimens was carried out by Frank Biancanello whose substantial contribution to this research is gratefully acknowledged. Assistance in the wear phases of the work from John Powell, Steven Bushby and David Cooper is also recognized.

REFERENCES

1. See for example, Proceedings of the International Conference on Metallurgical Coatings, 1980 (Elsevier Publ. Co., Oxford, U.K.).
2. See for example, Amorphous and Metastable Microcrystalline Rapidly Solidified Alloys: Status and Potential, National Materials Advisory Board, National Research Council, NMAI-358 (1980).
3. Breinan, E. M. and Kear, B. H., "Rapid Solidification Laser Processing of Materials for Control of Microstructure and Properties," in Rapid Solidification Processing: Principles and Technologies, ed. R. Mehrabian, B. H. Kear and M. Cohen (Claitors Publ. Div. 1978).
4. Glaeser, W. A. and Fairand, B. P., "Laser Surface Melting for Abrasion Resistance," Wear of Materials, 1979 (American Society of Mechanical Engineers, N.Y., 1979), p. 304-312.
5. Carpenter Matched Tool and Die Steels, (Carpenter Steel, Co. 1962).
6. Hogmark, S., Swahn, H. and Vingsbo, O., "A Specimen Preparation Technique for Transmission Electron Microscopy of Surface Layers," Ultramicroscopy 1, p. 113-120 (1975).
7. Metals Handbook: Heat Treating, Cleaning and Finishing, Vol. 2 (8th ed), (American Society for Metals, 1964).
8. Metals Handbook: Metallography, Structures and Phase Diagrams, Vol. 8 (8th ed.), (American Society for Metals, 1973).
9. Strutt, P. R. and Nowotny, H. Tuli, M. and Kear, B. H., "Laser Surface Melting of High Speed Tool Steels," Materials Science and Engineering 36.

p. 217-222 (1978).

10. Kim, Young-Mon, Strutt, P. R. and Nowotny, H., "Laser Melting and Heat Treatment of M2 Tool Steel: A Microstructural Characterization," Metallurgical Trans. 10A, p. 881-886 (1979). See also Strutt, P. R., Kurup, N. and Gilbert, D. A., "Comparative Study of Electron Beam and Laser Melting of M2 Tool Steel," Proc. Second Int. Conf. on Rapid Solidification Processing, 1980, ed. R. Mehrabian, B. H. Kear, N. Cohen (Claitors Publ. LA).

11. Ruff, A. W., Ives, L. K., and Glaeser, W. A., "Characterization of Wear Surfaces and Wear Debris," in Fundamentals of Friction and Wear of Materials, ed. D. A. Rigney (Am. Soc. Metals, to be published, 1980).

12. Budinski, K. G., "Wear of Tool Steels," Wear of Materials, 1977 (American Society of Mechanical Engineers, N.Y., 1977), p. 100-109.

13. Hirst, W., "Adhesive Wear," Engineering 8, 477 (1970).

14. Eyre, T. S. and Maynard, D., "Surface Aspects of Unlubricated Metal-to-Metal Wear," Wear 18, p. 301-310 (1971).

15. Landheer, D. and Zaat, J. H., "The Mechanism of Metal Transfer in Sliding Friction," Wear 27, p. 129-145 (1974).

16. Clayton, P., "The Relationships Between Wear Behavior and Basic Material Properties for Pearlitic Steels," Wear of Materials, 1979, (American Society of Mechanical Engineers, N.Y., 1979), p. 35-44.

TABLE 2
MICROHARDNESS AND GRAIN SIZE OF FLAT
SPECIMEN MATERIALS

Material	Average linear intercept Grain Size (μm)	Microhardness (Kg/mm^2) (Note 1)
OFHC Cu	13	44 \pm 6
Cu-15wt%Ag Cu-rich phase Eutectic areas	108 N/A	(Note 2) 148 \pm 14 (Note 2) 167 \pm 16
Cu-7.0wt%Al	15	106 \pm 15

Notes

- (1) Knoop indenter, 100 g (0.98 N) load, microhardness obtained by dividing load by projected area of indentation. Method given in Ref. [13].
- (2) Microstructure of Cu-Ag alloy consisted of two main constituents: a Cu rich phase (92 vol %) and a two-phase eutectic (8 vol %). To measure microhardness of individual constituents, a 10 g (0.098 N) load was used in this material.

TABLE 3
SLIDING TEST CONDITIONS

(Normal load 4.9 N, sliding velocity 0.5 cm/s)

Flat Specimen Material (wt%)	Run Code	Temp. ($^{\circ}\text{C}$)	Testing Environment of the Sliding Contact
OFHC Cu	A	24	Flowing Ar, 33 \pm 3%RH
	B	25	Laboratory air, 59 \pm 3%RH
	C	25	Constant immersion in distilled water
Cu-15Ag	D	25	Laboratory air, \pm 3%RH
Cu-7Al	E	24.5	Flowing Ar, 30 \pm 3%RH
	F	24	Laboratory air, 57 \pm 3%RH

Using plots of friction versus location, correlations between microstructures at and below wear tracks and frictional changes at given locations can be made. For example, Fig. 4 is an optical photomicrograph of a region about 1.6 cm from the starting end of the track of Cu slid in air (Fig. 3, top, and Fig. 8). Figure 5 is a metallographic taper section of the same sample at approximately the same location. Severe surface and subsurface material damage can be clearly observed. Together with other analytical techniques which measure surface chemistry, it may be possible to identify key mechanisms responsible for friction and wear behavior. At this writing such correlations are being performed on Cu alloys and steels at the National Bureau of Standards [14].

Figures 6, 7 and 8 represent the frictional "histories" for Cu-15wt%Ag, Cu-7wt%Al and OFHC Cu flats all tested in air with similar loads (4.9 N) and sliding velocities (0.5 cm/s). Each vertical scale unit is 0.1 of friction coefficient (μ) and the zero-friction base-lines for each successive stroke are indicated at the right side of the figures. By scanning the plots from bottom to top, one can observe the changes (or lack thereof) in friction at any point along the wear track. For example, the stroke by stroke change in

friction for a point 1.5 cm along the track of Fig. 8 has been plotted in Fig. 9. The usefulness of such formats lies in the study of microstructural contributions to wear and friction break-in behavior, since it is possible to examine structural features produced at locations with documented frictional histories.

One notes in such representations as Fig's. 6 through 8 that once certain features develop from stroke to stroke on a track, their influence may often aid in the further deterioration of the track. In Figure 8, for example, one might suggest that the plateau-shaped, high friction region developed on the last stroke may have arisen from material transfer to the rider ball surface at the "upstream" location indicated by the arrow. If a built up transfer film was formed so as to promote Cu-on-Cu sliding, one might expect to see higher friction, more effective load transfer to the flat, and therefore a greater potential for track deterioration. Sasada, et al [15] addressed this issue in a previous paper. Some of the plowed-up debris may have lead to adhesive removal of the transferred material at the end of the track so that the transfer process would need to be reinitiated on each subsequent stroke.

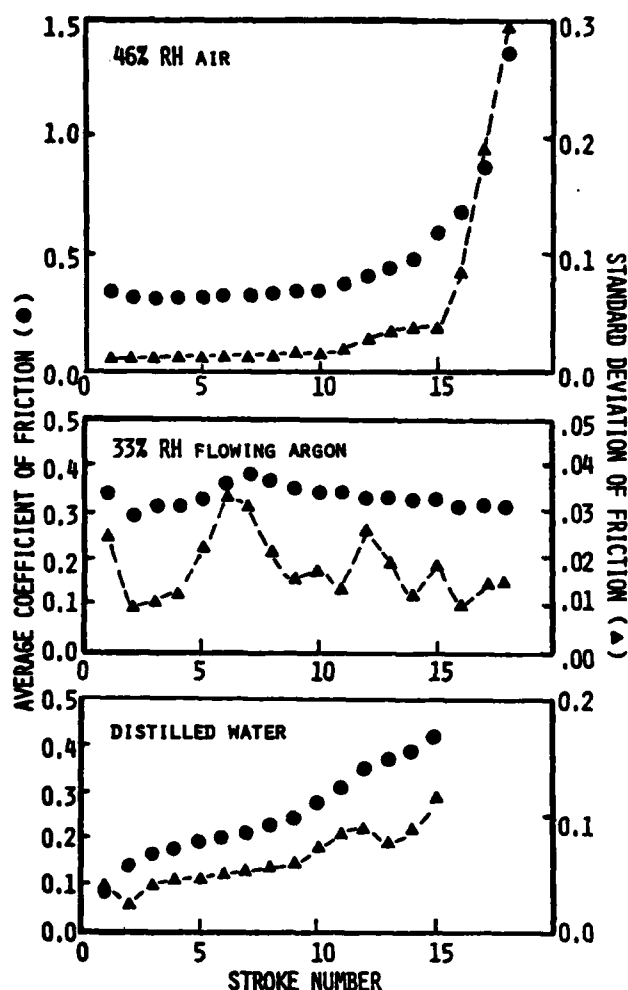


Fig. 3. Variations in the stroke by stroke frictional behavior of Cu in three sliding environments.

In contrast to Cu-15wt%Ag (Fig. 6) the Cu-7.0wt%Al alloy (Fig. 7) did not show the reproducibility of features or subsequent friction traces. This could indicate that substantially different wear surface features were produced at a given location during each stroke. Such observations can help to identify the extent to which the characteristics of prior wear surface influences longer term deterioration.

SUMMARY

This paper presented some preliminary findings of an on-going program to understand the contributions of microstructure and properties of Cu and its alloys to their behavior during the early stages of sliding. Measurement methods have permitted the collection of data relating to the frictional "histories" of

given locations on a wear track. Coupled with detailed microstructural observations, the role of microstructure in surface deterioration during wear eventually may be more clearly related to the mechanisms which give rise to sliding friction as well.

ACKNOWLEDGEMENTS

The author wishes to acknowledge the able assistance of E. Whinton, NBS, in electronic circuit design and computer software aspects of this work. The helpful discussions with A. W. Ruff, K. J. Bhansali and R. Polvani of NBS are also appreciated. This work was part of a program sponsored by the Office of Naval Research on microscopic aspects of wear in metals.

REFERENCES

1. P. J. Blau, "The Role of Metallurgical Structure in the Integrity of Sliding Solid Contacts," ASME Symposium on "Solid Contact and Lubrication," Chicago, ILL., Nov. 17-18, 1980.
2. J. T. Burwell and C. D. Stang, "On the Empirical Law of Adhesive Wear," *J. of Appl. Phys.*, Vol. 23, 1952, pp. 18-28.
3. D. F. Cornelius and W. H. Roberts, "Friction and Wear of Metals in Gases up to 600 C," *ASLE Trans.*, Vol. 4, 1961, pp. 20-32.
4. A. J. Haltner, "An Evaluation of the Role of Lubrication Mechanisms in MoS_2 ," *Wear*, Vol. 7, 1964, pp. 102-117.
5. R. Takagi and T. Liu, "The Lubrication of Steel by Electroplated Gold," *ASLE Trans.*, Vol. 10, 1967, pp. 115-123.
6. T. S. Eyre, R. F. Iles and D. W. Gasson, "Wear Characteristics of Flake and Nodular Graphite Cast Iron," *Wear*, Vol. 13, 1969, pp. 229-245.
7. R. M. Farrell and T. S. Eyre, "The Relationship Between Load and Sliding Distance in the Initiation of Mild Wear in Steels," *Wear*, Vol. 15, 1970, pp. 359-372.
8. R. S. Montgomery, "Friction and Wear Under Lubricated Reciprocating Sliding," *Wear*, Vol. 15, 1970, pp. 373-387.
9. H. Krause, "Tribological Reactions in the Friction and Wearing Process of Iron," *Wear*, Vol. 18, 1971, pp. 403-412.
10. S. Hogmark, O. Vingsbo and S. Fridstrom, "Mechanisms of Dry Wear of Some Martensitic Steels," *Wear*, Vol. 31, 1975, pp. 39-61.
11. P. J. Blau, "Interpretations of the Friction and Wear Break-in Behavior of Metals in Sliding Contact," submitted to *Wear*, 1980.
12. A. W. Ruff and P. J. Blau, "Studies of Microscopic Aspects of Wear Processes in Metals," NBSIR 80-2058, 1980, 72 pp.
13. P. J. Blau, "Use of a Two-Diagonal Measurement Method for Reducing Scatter in Knoop Microhardness Testing," *Scripta Met.*, Vol. 14, 1980, pp. 719-724.
14. A. W. Ruff and P. J. Blau, work in progress, National Bureau of Standards, Washington, DC, ONR contract N00014-79-F-0034, 1980.
15. T. Sasada, S. Norose and H. Mishina, "The Behavior of Adhered Fragments Interposed Between Sliding Surfaces and the Formation Process of Wear Particles," *Proc. Conf. on Wear of Materials*, Dearborn, Mich., 1979, pp. 72-80.

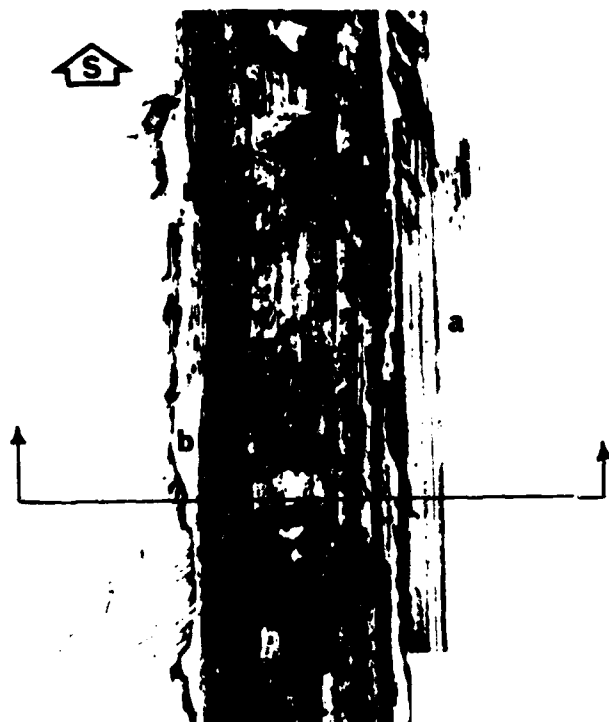


Fig. 4. Optical photomicrograph of a wear track on Cu tested in air. (Data for this test given in Fig. 3 (top) and Fig's 8 and 9). Sliding direction given by the arrow.



Fig. 5. Polished cross-section of the track in Fig. 4. Inclining the plane of polish produced enhanced magnification of surface features and subsurface deformation. Areas of mild scoring (a) and a raised lip (b) correspond to Fig. 4 features.

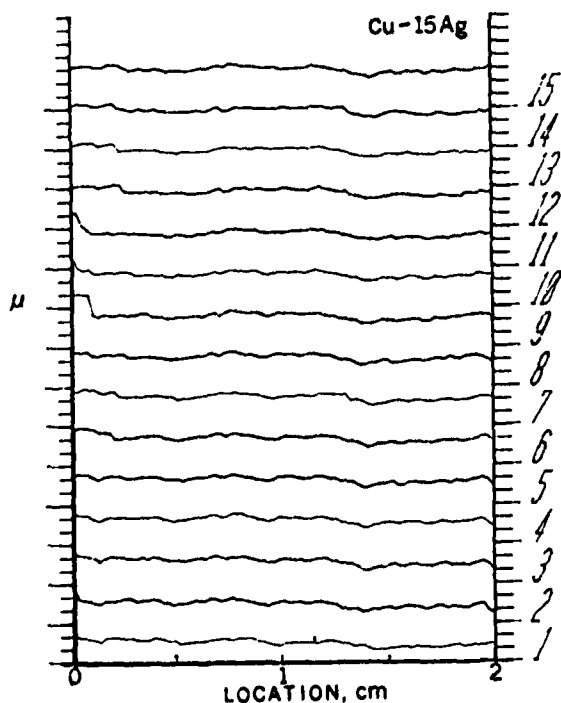


Fig. 6. Wear history of a Cu-15%Ag (in air) specimen showing little variation in friction and similar behavior from one stroke to the next.

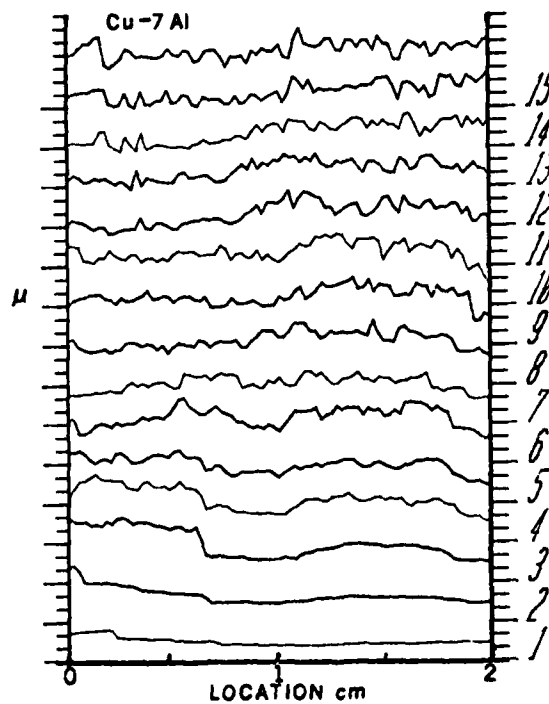


Fig. 7. Rapid, early transition from low steady friction to higher, more erratic friction in a Cu-7%Al alloy (in air).

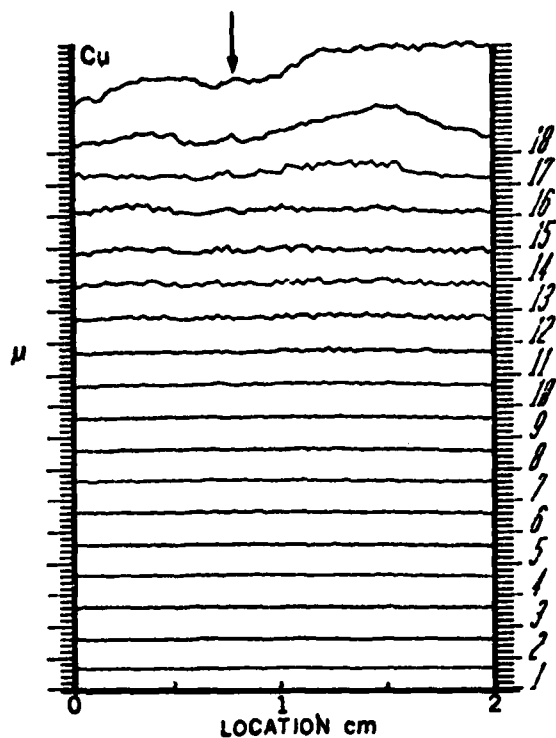


Fig. 8. Small localized frictional variations precede a large transition in friction in a test of Cu in air. Higher friction at the right end of the track may result from metal transfer to the slider after about the first cm of travel.

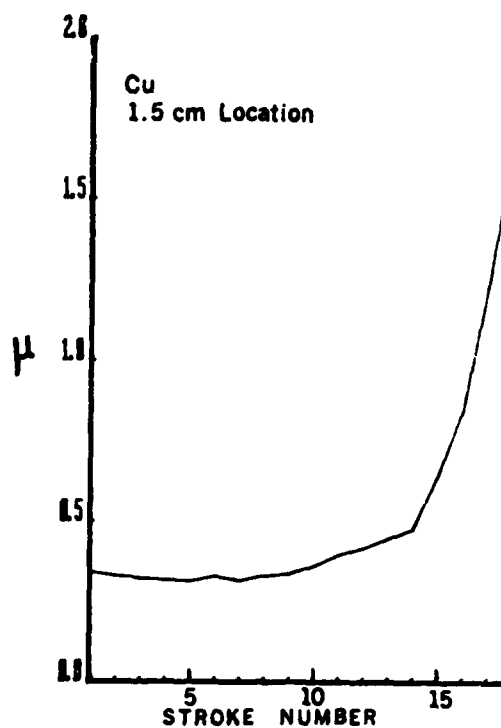


Fig. 9. Change in friction from stroke to stroke for a point 1.5 cm down the wear test track, Fig. 8. Most rapid changes occurred during strokes 14 to 18.

reprinted from

Wear of Materials - 1981

Edited by S.K. Rhee, A.W. Ruff and K.C. Ludema

published by

THE AMERICAN SOCIETY OF MECHANICAL ENGINEERS

345 East 47th Street, New York, N.Y. 10017

Printed in U.S.A.

OBSERVATIONS ON THE WEAR-IN PROCESS DURING THE SLIDING OF SEVERAL COPPER ALLOYS AGAINST 52100 STEEL

P. J. Blau
Metallurgy Division
National Bureau of Standards
Washington, D. C.

ABSTRACT

The changes in the surface and subsurface microstructures which occur in early stages of metal sliding contact may set the stage for longer term friction and wear behavior. The current paper presents the results of a study of the friction and wear break-in behavior of Cu, Cu-7wt%Al, and Cu-15wt%Ag rubbing against fixed 52100 steel ball bearing sliders in a stroke-by-stroke linear wear test device. Friction was measured at 81 locations on each wear track and plotted by computer to reveal the frictional "histories" of the given locations. The development of variations in the frictions traces was correlated with microstructure of the worn tracks to clarify the effects of previous sliding history on surface deterioration in the tested materials. Sliding behavior in air, flowing argon and distilled water was reported for Cu.

INTRODUCTION

When solid surfaces are first brought into contact and slid relative to one another a complex process leading to surface deterioration in one or both solids begins to occur (Fig. 1). Some of the interpretations of the transient friction and wear behavior during early stages of sliding have been discussed in the literature (e.g. Ref [2-11]) but it is clear that much more work in this area is needed before the possible effects of the many candidate mechanisms can be incorporated

to apply to any given break-in situation. The current paper reports on the results of an investigation which has focused on the microstructural aspects of the wear-in process in copper and two of its alloys. In particular, the frictional "history" of selected portions of wear tracks are related through metallography to the microstructures produced by sliding. Effects of material properties and environment during sliding produced quite different frictional histories and wear scar appearances from track to track.

MATERIALS

Table 1 lists the compositions and thermomechanical treatments given to the materials which were used in this investigation. In addition, Table 2 gives the average pre-test microhardness and grain sizes of the test materials.

TEST METHOD

The tribometer used for the current studies was computer controlled and operated in a linear, stroke-by-stroke fashion [12]. Figure 2 represents the basic test geometry. Friction forces were measured using a strain ring which was calibrated before each test and monitored for signal stability and drift between each stroke during the test. The current series of tests were all conducted using a fixed 52100 steel ball bearing rider (0.635 cm in diameter) with a load of

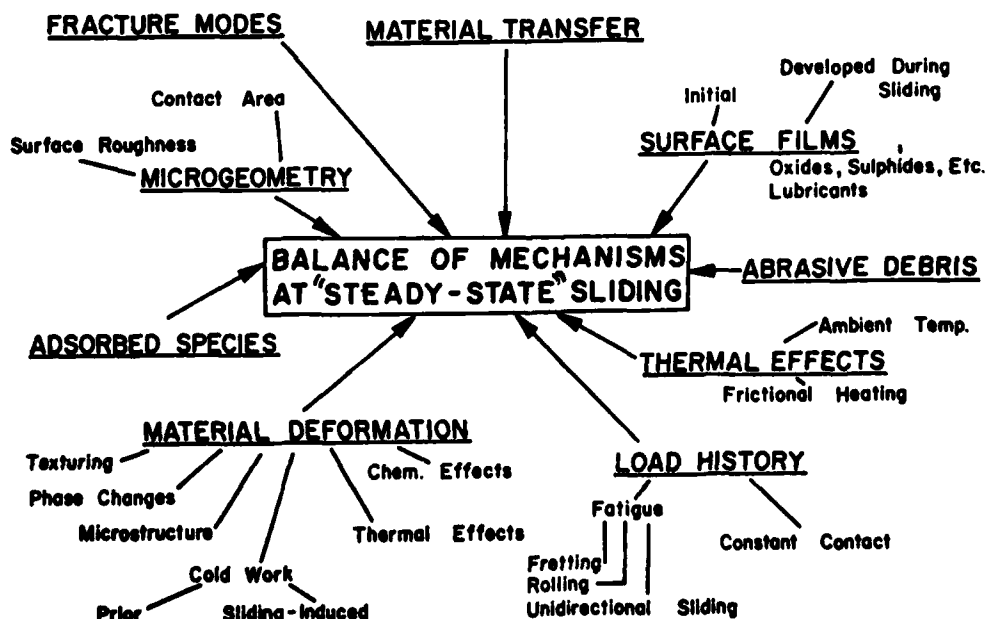


Fig. 1. Summary of several of the many possible mechanisms contributing to sliding behavior (from Ref. [1]).

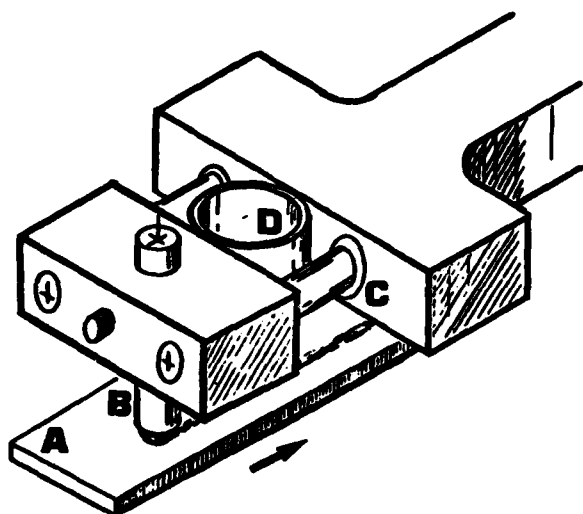


Fig. 2. Schematic of the linear tribometer head: (A) specimen, (B) ball rider on a brass stub, (C) precision linear ball bushing, (D) strain ring with gauges.

500 g (4.9 N) and a sliding speed of 0.5 cm/s. Stroke length was 2.0 cm and 81 values of frictional force were recorded for each stroke. In this way, friction was recorded as a function of rider position at 0.25 mm intervals along the wear track.

Sliding materials were cleaned in acetone and methanol immediately before testing. In addition, the flat samples were freshly final-polished using a 1 μ m diamond lap within about 1 hour of the test. Sliding conditions for the various test runs are listed in Table 3.

RESULTS AND DISCUSSION

Figure 3 demonstrates the manner in which the averages and standard deviations of the kinetic friction coefficients changed from stroke to stroke in three sliding tests for Cu. Each plotted point represents a sampling of 81 values measured at 0.25 mm intervals along the 2.0 cm long sliding track. The three runs exemplify environmental effects on frictional break-in's. For the run in air, there was a rapid increase in both average friction and standard deviation of friction over a period of only about four strokes once severe wear-in began; whereas, for the lower humidity run, average friction changed little while the standard deviation varied erratically from stroke to stroke. When rider and flat were tested in distilled water, both the average friction and standard deviation gradually increased. Interpretation of these results and others like them must address many possible environmental interactions, including for example:

- 1) material transfer from one component to another and back again.
- 2) formation and action of surface films of various types.
- 3) debris removal processes (including fluid transport).
- 4) surface and subsurface microstructural behavior.

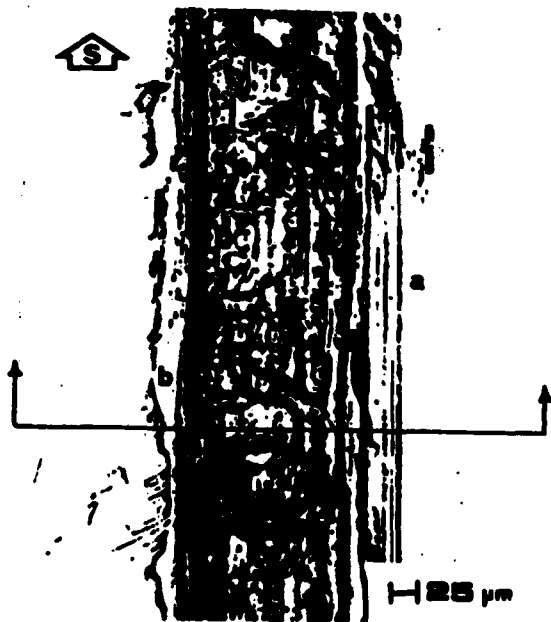
While data such as that in Fig. 3 can provide useful information about general trends in friction and wear mode transitions in given sliding systems, to identify the fundamental mechanisms, more detailed knowledge about the evolution of surface damage is needed. To this end, the appropriate computer software was written to plot kinetic friction versus location on the wear track for each subsequent pass of the slider.

TABLE 1
MATERIAL COMPOSITIONS AND PREPARATION

Material	As-received Form	Thermomechanical Treatment
Oxygen-Free, High conductivity Cu	Extruded rod	Annealed 4 hrs. at 535°C in vacuum
Cu-15wt%Ag	Lab melt	Melt in vacuum; quench; cold roll about 50%; anneal in vacuum 2 hrs. at 740°C; then 16 hrs. at 845°C; quench
Cu-7.0wt%Al	Warm-rolled plate	Cold roll 50%; anneal 4 hrs. at 535°C in vacuum; quench

REPRINT ERRATA - Wear of Materials 1981, pp. 69-74
P. J. Blau

- 1) Table 3 - Cu-15Ag "58 \pm 3%RH"
- 2) Reference 11 - "to be published 1981"
- 3) Fig. 4 and 5 - micrometer markers as below:



END

FILMED

10-84

DTIC